Journal of the Serbian Society for Computational Mechanics / Vol. 17 / No. 1, 2023 / pp 111-124
(10.24874/jsscm.2023.17.01.08)

THE ANEURISMAL ABDOMINAL AORTA WALL MECHANICAL RESISTANCE LOSS AND COLLAGEN FIBRE PATHOLOGICAL REORIENTATION - A NUMERICAL STUDY

Bouteraa Samira[1]*, Bouaricha Amor[2], Zemouri Zahia[1] and Berkani Mahièddine[3]

[1] Research Laboratory of Industrial Risk, Control, and Security, Faculty of Technology, Badji Mokhtar University, Annaba, Algeria
e-mail: samirabout1992@gmail.com
[2] Industrial Mechanical Laboratory. Faculty of Technology, Badji Mokhtar University, Annaba, Algeria
e-mail: bouarichaa@yahoo.fr
[3] Research Laboratory of Electromechanical Systems, Faculty of Technology, Badji Mokhtar University, Annaba, Algeria
e-mail: m_berkani@yahoo.fr

Abstract

The biomechanical properties' changes of the abdominal aortic aneurysms' (AAA) walls are closely related to the pathological degeneration of the smooth muscle cells and the main fibrous components (collagen and elastin). In this study, the passive mechanical response of the aneurysmal aortic wall is computationally investigated as a function of the dispersion and orientation of collagen. So, to better understand how the ultimate resistance of the diseased wall varies, several numerical simulations on models of AAA specimens have been performed, using the Gasser-Ogden-Holzapfel anisotropic hyperplastic constitutive model where the dispersion and orientation parameters are explicitly introduced. The simulations were carried out for a variation of the average orientation of the collagen from 0° to 90° with a dispersion that varies from 0 (orthotropic case) to 1/3 (isotropic case). The results of the numerical simulations show that an increase in the dispersion and the angle of orientation in the aneurysm leads to a decrease in the circumferential resistance of the diseased artery. Such results can help to better understand the negative effects of the disease on the arterial wall and to target the necessary therapy.

Keywords: Abdominal aortic aneurysms, Xenograft rat model, collagen fibre dispersion, collagen fibre orientation, constitutive model.

1. Introduction

Arterial aneurysms (AA) such as intracranial aneurysm (IA) or abdominal aortic aneurysm (AAA) are degenerative diseases that manifest as localized enlargement of the artery. If not treated, the IA or AAA may grow slowly and irreversibly until rupture when wall stress is locally higher than the aneurismal wall strength (Fillinger et al. 2003). AAA rupture causes a high mortality rate of 90% (Sakalihasan et al. 2005). Often, AA is associated with the development of an intraluminal thrombus (Dobrin, 1989). The idealized architecture of an arterial vessel is

cylindrical, and composed of three distinct layers: intima (inner layer), media (middle layer) and adventitia (outer layer). The media layer is the most load-bearing layer in physiological conditions of blood pressure. So, the media tissue is mainly made of elastin and collagen fibres imbibed in basic substance of smooth muscle cells (SMC) (Tsamis et al. 2013). In healthy cases, unlike elastin which remains stable with age (lifetime of about 50 years), collagen fibre (CF) is in continuous synthesis and degradation (Fonck et al. 2007; Wang et al. 2006). CF is stiffer than elastin fibre (EF). At physiological low blood pressure, the EFs bear most of the load while the CFs remain wavy and crimped. As the blood pressure increases, CFs are gradually recruited to become straightened to associate with the elastin to prevent any excessive expansion (see Fig. 1). The structural components of media guarantee the mechanical properties and integrity of the healthy arterial wall (Watton et al. 2009). Abdominal aortic aneurysm (AAA) is a disease that occurs usually in the elderly and results from a progressive decrease in SMC density associated with proteolytic defragmentation of elastin against an increase in the density of CF according to Sakalihasan et al. (2005), Zidi et al. (2014) and Niestrawska et al. (2016).

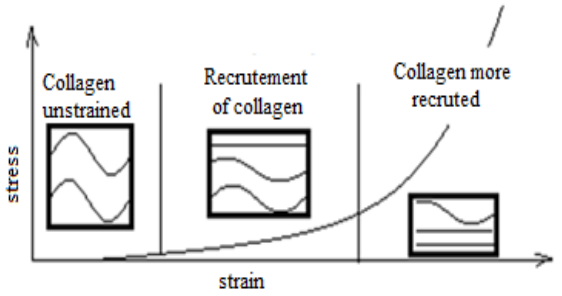

Fig. 1. Mechanical responses of collagen fibre under straining.

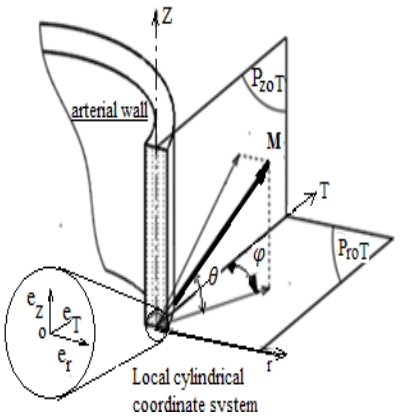

Fig. 2. Definition of an arbitrary orientation $\mathbf{M}_i$ of fibre direction. $\mathbf{M}_i$ is defined by means of Eulerian angles (e_r, e_T, e_Z). e_r, e_T, e_Z represent the unit vectors of the principal basis. P_{roT} is the radial plane, P_{ZoT} is the tangential plane.

This leads to geometric and structural remodelling such as the outer diameter of the artery becomes larger and the CFs become straight and unrippled with a new spatial orientation (see Fig.1). The microstructural rearrangement, particularly of the CFs explains why the artery

becomes stiffer and weak in circumferential direction than longitudinal (Xiong et al. 2009), (Zidi et al. 2014). However, the loss of elastin in the structural composition of the aneurismal tissue is not the sole cause of its weakness but the numbers of collagen and their spatial orientation also have their role in this problem. Vande Geest (2006) and Niestrawska (2016) have shown that the CF reorientation (θ) in AAA becomes widely more dispersed in the circumferential plane (e_T, e_Z) than in the radial one without significant identified difference between medial and adventitial layers (see Fig.2). So, this study is limited to a plane (e_r, e_T) of the media as a single layer reinforced with CFs (see Fig.2 and Fig.3).

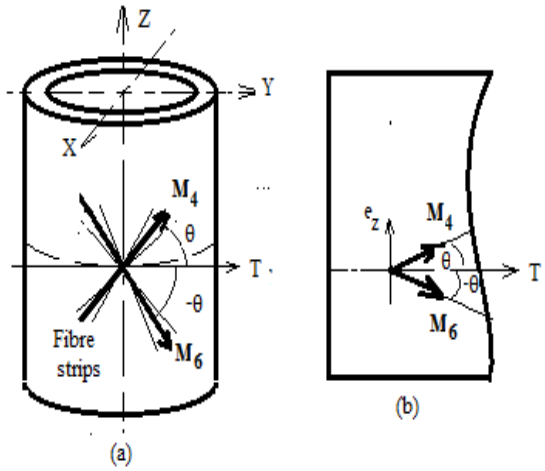

Fig. 3. Geometrical modelization of disposition in tangential plane $P_{ZoT} = (e_T, e_Z)$ of undeformed tubular tisssue layer. (a)- $(\mathbf{M}_4, \mathbf{M}_6)$ Mean orientations of CFs families. (b). - a lamella of media in the plane $(\varphi = 0)$ with two symmetrically disposed families with $\mathbf{M}_4$ and $\mathbf{M}_6$ directions in the reference configuration (undeformed state). (X, Y, Z) assumed as principal axes. The reference system (e_r, e_T, e_Z) is obtained by translation of (X, Y, Z).

The studies of Gasser et al. (2006) and Niestrawska et al. (2016) investigated the mechanical effects of the symmetric fibre dispersion (κ) on the risk of rupture of arterial wall that is transversely isotropic, but, to the best of the author knowledge, only the effects of dispersion (κ) variations have been studied without any indication of the fibre orientation which is generally variable from case to case. Moreover, the aneurysmal wall rupture is mainly due to the tangential component of stress field generated by blood pressure (Ayyalasomayajula et al. 2023; Zidi et al. 2014; Hariton et al.2007; Di Martino et al. 2006). Therefore, to show the effects of the orientation and dispersion parameters of the CFs on the arterial wall resistance, this study is limited to determine the tangential component of the stress field generated by the blood pressure.

For this purpose and to fully explain the steps followed in this paper, the following paragraphs include an explanation on how the characteristics (dispersion κ and orientation θ) of the aneurysm intervene in the arterial tissue behavior. Another paragraph dedicated to the numerical calculation explains how the numerical modelling is carried out and the generated stress fields $\boldsymbol{\sigma}$ were obtained. The results of the numerical simulations are presented in the form of circumferential stress-dispersion or stress-orientation angle of the CFs curves.

2. Methods

Because the results of this paper would constitute a future platform to study the response of AAA tissue to cell therapies, the geometric data used to develop the numerical simulations were taken from the experiments carried out to create AAAs according to the xenograft model in the rat (Zidi et al. 2014).

2.1. Modelling and numerical approach

In this study, the tunica media as proposed by Niestrawska et al. (2016) is single layer and fibre-reinforced composite. So, the media layer is assumed to consist of a homogeneous non-collagenous matrix linked to an embedded collagenous reinforcement and arranged as two fibre symmetrical families**.** A mean orientation $\mathbf{M}_i$ $(i=1,2)$ of each fibre family is defined by Eulerian coordinates (θ,φ) shown in Fig. 2 and Fig. 3.

So, in the undeformed state, the orientation vector $\mathbf{M}_i$ is given by**:**

$$\mathbf{M}_i = \cos\theta.\sin\varphi\mathbf{e}_r + \cos\theta.\sin\varphi\mathbf{e}_T + \sin\theta\mathbf{e}_z \; ; \theta \in \left[-\frac{\pi}{2},+\frac{\pi}{2}\right]; \; \varphi \in [0,2\pi], \; (i=1,2) \tag{1}$$

The media is considered without a significant radial component of $\mathbf{M}_i$, then $\mathbf{M}_i$ in P_{ZoT} plane will be simplified as:

$$\mathbf{M}_i = \cos\theta\mathbf{e}_T + \sin\theta\mathbf{e}_z \tag{2}$$

For $\theta = 0^\circ$ or $\theta = 90^\circ$ the CFs are respectively circumferential or longitudinal.

For the purpose of this paper, we can cite several studies that have used. Among them, on can cite the works of Gasser (2006), Zulliger (2007), and Rodríguez (2008). The mechanical behaviour of the diseased abdominal aortic wall is assumed as composite axisymmetric, hyperelastic, incompressible, nonlinear and anisotropic material (Gasser et.al. 2006; Polzer et al. 2013; Justyna et al. 2018). So, to better describe the random mechanical contribution of collagen density in the $\mathbf{M}_i$ direction, the dispersion parameter κ, according to Gasser (2006) was introduced into the mechanical behaviour model of the aorta that is characterized by the strain energy density function (W). The model of Gasser currently called Gasser - Ogden- Holzapfel (GOH) model is adopted with two fibre families (Holzapfel et al. 2000) where the mechanical contribution of the CFs in load bearing is defined by the dispersion parameter κ [-] in the plane (e_T, e_Z) that can be either rotationally symmetric or perfectly aligned according to $\mathbf{M}_i$ direction. According to the contribution of each structural component of the tissue, the GOH model W can be decoupled as follows:

$$W = W_{iso} + W_{aniso} \tag{3}$$

W_{iso}, characterizes the isotropic Neo-Hookean behavior of the non-collagenous matrix and the anisotropic exponential function W_{aniso} representing the contribution of the collagen matrix:

$$W_{iso} = \frac{c}{2}(I_1 - 3) \tag{4}$$

$c[MPa] > 0$ Young's modulus of the non-collagenous matrix in the reference configuration.

W_{aniso} is function of strain Cauchy Green tensor ($\mathbf{C}$) where the fibre stretch is defined by the pseudo-tensors (I_4 and I_6) and the dispersion parameter κ . Explicitly, W_{aniso} as developed by Gasser (2006) can be given as follows:

$$W_{aniso} = W_{aniso}\left(C, I_4, I_6, \kappa\right) = \frac{1}{2}\Sigma_{i=4,6}\left\{\frac{k_{1,i}}{k_{2,i}}\left[\exp\left[k_{2,i}\left(\kappa I_1 + \left(1-3\kappa\right)I_i - 1\right)^2\right] - 1\right]\right\}; i = 4,6 \quad (5)$$

$\mathrm{I}_1 = \left(\lambda_\mathrm{r}{}^2 + \lambda_\mathrm{T}{}^2 + \lambda_\mathrm{Z}{}^2\right) = \mathrm{tr}\left(\mathrm{C}\right)$, is the first invariant of Cauchy Green tensor ($\mathbf{C}$) expressed by:

$$\mathbf{C} = \mathbf{F}^\mathrm{T}\mathbf{F} \quad (6)$$

$\lambda_r, \lambda_T, \lambda_Z$ are respectively the radial, tangential and longitudinal principal stretches in undeformed configuration $\mathbf{F}$, $\mathbf{F}^\mathrm{T}$ are the gradient of deformation and its transpose. $\mathbf{F}$ is given by the following equation:

$$\mathbf{F} = diag\left(\lambda_r, \lambda_T, \lambda_Z\right) \quad (7)$$

Each CF is considered as a one-dimensional mechanical entity oriented according to the tension direction ($\mathbf{M}_i$) Its elongation (λ_{fi}) in $\mathbf{M}_i$ direction is:

$$\lambda_{fi}{}^2 = \mathbf{m}_i^T\mathbf{m}_i \;\; ; \;\; \mathbf{m}_i = \mathbf{F}\mathbf{M}_i \; ; \; i = 1,2 \quad (8)$$

In the adopted GOH constitutive model, the mechanical contribution of CFs density and their orientation $\mathbf{M}_i$ is characterized through the anisotropic strain invariant I_i $\left(i = 4,6\right)$ and the dispersion parameter κ . I_i indicates the fibre elongation according to $\mathbf{M}_i$ direction. It is given by:

$$I_4 = \mathbf{M_4^T}\left(\mathbf{CM_4}\right) = \left(\lambda_{f4}\right)^2 \text{ and } I_6 = \mathbf{M_6^T}\left(\mathbf{CM_6}\right) = \left(\lambda_{f6}\right)^2 \quad (9)$$

λ_{f4} and λ_{f6} are the elongations in the undeformed configuration, according to the symmetrical directions $\mathbf{M}_4$ and $\mathbf{M}_6$ respectively. As mentioned before, since the CFs are crimped excepted when they are subjected in tensile, the structural invariants I_i must check the conditions: $I_4 > 1$ and $I_6 > 1$. In the present work, the elongation of the CFs takes place according to its variable orientation from $\theta = 0°$ to $\theta = 90°$. Finally, it is clear to understand that the aneurysmal tissue behaviour depends of $\mathbf{M}_i$ direction and dispersion κ , see equations (3) and (5). κ describes the symmetrical dispersion degree of anisotropy. For instance, when $\kappa = 0$, all fibres of the family are aligned in the same privileged direction $\mathbf{M}_i$, that is the anisotropic case. Whereas, when $\kappa = \frac{1}{3}$, the CF directions are uniformly dispersed (without any privileged direction), that is the isotropic case. Then, to know how the density of the fibres in any direction θ influences the mechanical response, in the numerical simulations, κ is considered variable from the isotropic state of the fibres in any direction θ influences the mechanical response, in the

numerical simulations, κ is considered variable from the isotropic state $\left(\kappa = \frac{1}{3}\right)$ to the orthotropic state $\kappa = 0$.

The dispersion of the fibre orientation in each fibre family of the unilayer composite media is taken into account in the constitutive model as W :

$$W = \frac{c}{2}(I_1 - 3) + \frac{1}{2}\Sigma_{i=4,6}\left\{\frac{k_{1,i}}{k_{2,i}}\left[\exp\left[k_{2,i}\left(\kappa I_1 + (1-3\kappa)I_i - 1\right)^2\right] - 1\right]\right\} \quad (10)$$

The material parameters $(c, k_{1,i}, k_{2,i})$ of aneurismal tissue are adopted from calibrating the GOH model to the mechanical data obtained from testing on mice arterial tissues in Karimi (2015).

Assuming symmetrical families of the fibre reinforcement ($I_4 = I_6$) with same mechanical properties $\left(k_{1,4} = k_{1,6} = k_1 and\, k_{2,4} = k_{2,6} = k_2\right)$ and same dispersion in the AAA tissue, the mechanical anisotropic contribution of the two families becomes:

$$W_{aniso} = \frac{k_1}{k_2}\left[\exp\left[k_2\left(\kappa I_1 + (1-3\kappa)I_4 - 1\right)^2\right] - 1\right] \quad (11)$$

The structural parameters κ , and θ in W_{aniso} can be determined for example by structural analysis based on the second-harmonic generation imaging (Niestrawska et al. 2016; Justyna et al. 2018). In this study, W can be given explicitly by:

$$W = W(c; k_1, k_2, \theta, \kappa) = \frac{c}{2}\left(\lambda_T{}^{-2}\lambda_Z{}^{-2} + \lambda_T{}^2 + \lambda_Z{}^2 - 3\right) + \frac{k_1}{k_2}\left[\exp\left[k_2\left[\kappa\left(\lambda_T{}^{-2}\lambda_Z{}^{-2} + \lambda_T{}^2 + \lambda_Z{}^2\right) + (1-3\kappa)\left(\lambda_T{}^2\cos^2\theta + \lambda_Z{}^2\sin^2\theta\right) - 1\right]^2\right] - 1\right] \quad (12)$$

For the arterial tissue, Cauchy stress tensor ($\boldsymbol{\sigma}$) can be obtained by deriving W as:

$$\boldsymbol{\sigma} = -p\mathbf{I} + \mathbf{F}\frac{\partial(W)}{\partial C}\mathbf{F}^T \quad (13)$$

Where $\mathbf{I}$ is the identity matrix, p is the Lagrange multiplier which can be analytically determined respecting the incompressibility hypothesis ($\lambda_r, \lambda_T, \lambda_Z = 1$) and the plane stress state ($\sigma_{rr} = 0$). p can be given by:

$$p = c\lambda_{rr}^2 = c\lambda_T^{-2}\lambda_Z^{-2} \quad (14)$$

All components of $\boldsymbol{\sigma}$ are given by deriving $W(c; k_1, k_2, \theta, \kappa)$ as shouwn in equation (13).

From experimental observations reported in Watton (2009), He (1994), Vande Geest (2006), Zidi (2014), Djellouli (2017) and Lindeman (2010); the aneurism pathology decreases the resistance in circumferential direction of the AAA wall and, as above mentioned, the tangential macroscopic stress σ_T is often the most likely to cause the rupture of the aneurysm wall, so, the simulations of the present finite element analysis are focused on the evolution of σ_T for all

possible variations of the CF dispersion κ and the average orientation θ. Therefore, two approaches have been adopted.

The first approach consists in numerically computing the circumferential stress $\sigma_{T_k}(\theta,\kappa_k);(k=1,2,3,4)$ as a functions of κ; $\left(\kappa_1=0,\kappa_2=\frac{1}{9},\kappa_3=\frac{2}{9},\kappa_4=\frac{1}{3}\right)$, with θ taken invariable.

In the second approach, computing the circumferential stress $\sigma_{T_k}(\theta_k,\kappa),(k=1,2,3,4)$ is carried out for all values of θ; $(\theta_1=0^\circ,\theta_2=30^\circ,\theta_3=60^\circ,\theta_4=90^\circ)$, with κ taken invariable for this case. The values of θ and κ are taken arbitrarily and may not reflect the reality of the microscopic structure of the aneurysmal tissue.

The numerical simulations are carried out for all values of κ and θ that have been successively incorporated in GOH model (see equations (9) and (10). From the results of both approaches, according to θ and κ, it is possible to deduce the optimal values of κ and θ which provide the necessary information on the rupture risk of the aneurysmal tissue.

2.2 Geometry of finite element model

The geometric model used in the numerical simulations which is schematized in Fig. 5b was rebuilt starting from the elliptical profile $r(z)$ (Fig. 4) from the data given in Table.1. The elliptical profile $r(z)$ of the AAA curve is achieved using Matlab R2015a (Mathworks Inc., USA). The 3D model of AAA is designed using a Solidworks software as shown in Fig. 6a.

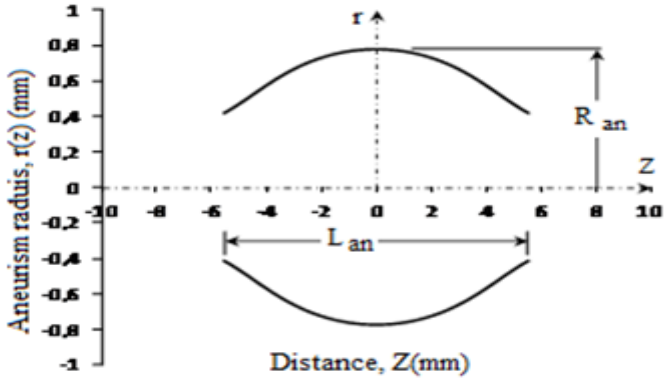

Fig. 4. External aneurism profile $r(z)$ (Matlab Results).

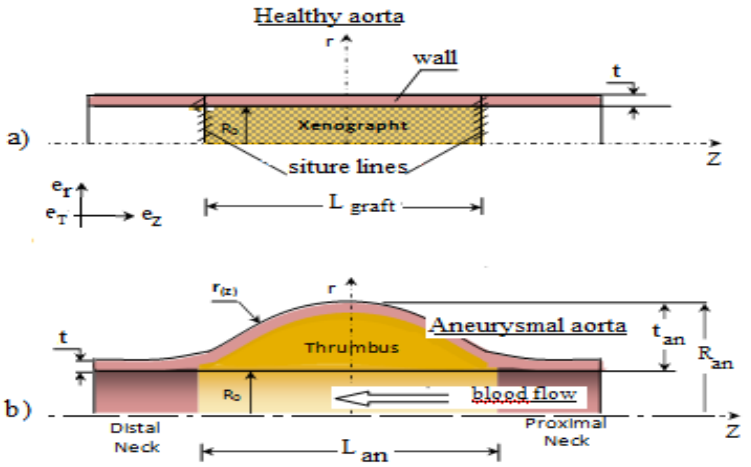

Fig. 5. Reconstruction of geometrical models.5a- the xenograft of decellularized aorta of male guinea pig transplanted orthotropically in rat (as defined in the xenotransplantation protocol (Djellouli et al. 2017). 5b- the reconstructed geometrical model of obtained AAA at fourteen days (D14) after xenotransplantation. AAA thickness t_{an} includes the thicknesses of aorta (t) assumed unchanged and thrumb.

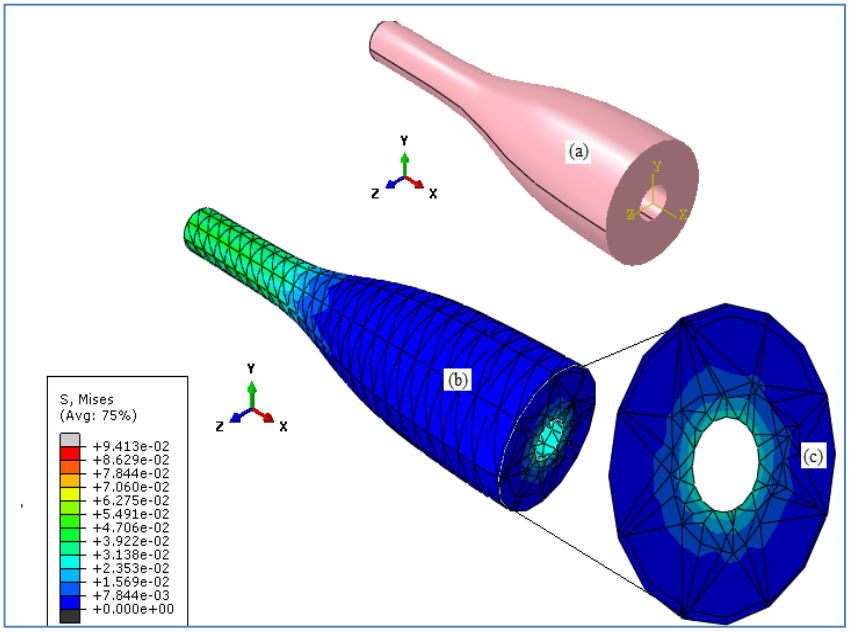

Fig. 6. Geometry of 3D model AAA used in numerical simulations. a- AAA views from outside of half geometric model with external generating line; b- meshing of half geometric model; c- stress field and its evolution through the redial thickness of the aneurysm.

The geometrical parameters of healthy aorta and AAA have been recorded respectively before xenotrans plantation (corresponding at time (D0)) and after 14 days later (D14) when the aneurism is created as recommended by the protocol of experimentation. (Zidi M. et al. 2014)

Parameters	Designation	Value = Mean ± SD (mm)
R_0	Internal Radius of Healthy aorta (D0)	0.588±0.03
R_{an}	Aneurismal Radius (D14)	1.55±0.05
r(z)	Aneurismal profile raduis at distance z	
T	Wall thickness (D0)	0.242 ±0.22
t_{an}	Wall thickness of the aneurismal profile*	0.962±0.07
L_{graft}	Length of sutured graft	7.72 ±0.63
L_{an}	Aneurismal length	11.05±0.52
*The wall thickness of the aneurismal represents the sum of thrombus and healthy wall thicknesses. p = 0.021 Mann–Whitney U test for % of variation (p< 0.05).		

Table 1. Geometrical parameters used in the reconstruction of (AAA) model.

The external profile $r(z)$ of the aneurysm is expressed by following equation:

$$r(z) = R_0 + \left[\left(\left(R_{an} - R_0\right) - c_3 \frac{z^2}{R_0}\right)\exp\left(-c_2 \left|\frac{z}{R_0}\right|^{c_1}\right)\right] \tag{15}$$

Where: $\left(-\frac{L_{an}}{2} < z < \frac{L_{an}}{2}\right)$; $c_2 = \frac{4.605}{\left(0.5L_{an}/R_0\right)^{c_1}}$; $c_3 = \frac{R_{an} - R_0}{R_0\left(0.8L_{an}/R_0\right)^2}$

$c_1 = 3.10^{-6}[-], c_2[-]$ and $c_3[-]$ are dimensionless scalar functions which are determined for the geometric data L_{an}. The investigation of the aneurismal tissue weakness resulting from aneurismal remodelling has been carried out on the reconstructed geometrical models of AAA with the mechanical properties of aneurismal tissue assumed obtained at (D14). The analysis by finite element method concerns the geometric models of the AAA for all values of θ and κ.

2.3. Numerical computation

Numerical computation of stresses has been carried out by using the commercial finite element software ABAQUS/CAE 2014, Dassault Systemes SIMULIA Corp. It has been conducted under static blood pressure P=16kPa corresponding to systolic pressure.

The boundary conditions are as follows:

- while the distal neck has been blocked according the z direction, the displacement $\lambda_Z = 0$ and, to take into account the action of the renal arteries, the proximal neck is undergoing an average imposed stretch of $\lambda_Z = 1.15$.
- In the radial plane $(\mathbf{e}_r, \mathbf{e}_T)$, the expansion is free, while to avoid rigid displacement, one single generation line of the aneurysm envelope is blocked in the longitudinal plane $(\mathbf{e}_T, \mathbf{e}_Z)$. In Fig. 6a the plane $(\mathbf{e}_r, \mathbf{e}_T)$ corresponds to the (x,y) plane and $(\mathbf{e}_T, \mathbf{e}_Z)$ to (y,z).

The analysis is performed on the 3D geometry that is discretized in 1045 quadratic hybrid tetrahedron (C3D10H) elements, (see Fig. 6b). The mechanical properties given in the following

Table 2 are used. The aneurism thickness t_{an} represents the sum of the thrombus thickness and the healthy wall thickness which form a single material (see Fig. 5b).

material parameters of the Abdominal aorta				
	c (kPa)	k_1(kPa)	k_2(-)	R^2
Healthy aorta	11.59	2.66	19.25	0.89
AAA	16.08	11.68	07.18	0.98

Table 2. Material parameters of the AAA samples adopted and calibrated from biaxial stretching tests (Niestrawska et al. 2016).

3. Results and discussion

An investigation on the effect of the orientation θ of the CFs in the AAA wall has been conducted using FEM in large deformations. Firstly, the geometrical model of AAA (Fig.6a) has been developed on the basis of geometrical measures collected during aneurism creation tests in rat (Djellouli et al. 2017) and generated from the external AAA envelop profile $r(z)$ computed by Matlab software. Secondly, the 3D geometry model of AAA is generated and obtained from $r(z)$ by using Solidworks software.

Finally, to asses numerically the stress (σ_T), numerical simulations have been conducted, based on the adopted GOH model that is favourite to be able to capture density and spatial distribution of the collagen fibre orientation. The parametrical calculations have been conducted for all values of independent variables (θ) and (κ).

From numerical results, the evolution of $\sigma_T = \sigma_T(\theta, \kappa)$ is plotted for CFs mean orientation θ, variable from 0° to 90° as shown on Fig.7.Thes curves corresponds to different values of statistical distribution parameter κ ; $(\kappa = 0, \frac{1}{9}, \frac{2}{9}, \frac{3}{9})$

When all CFs $(\kappa = 0)$ are oriented according to circumferential direction $(\theta = 0^\circ)$, the maximum value of the circumferential stresses (σ_T) means that the tissue is of a highest level of strength. As the orientation angle θ increases, σ_T decrease implying that the tissue becomes increasingly week. The highest level of strength is recorded at $(\theta = 0^\circ)$, when $(\kappa = 0)$ (orthotropic case of tissue). This situation cannot be that of an aneurysmal tissue.

It must be noted that when θ increases, the contribution of CFs in circumferential resistance of diseased tissue diminishes to vanish when $\theta = 90^\circ$, at this stage only the isotropic basic tissue (cellular matrix) bears the circumferential load. This case is also observed when the CFs are uniformly distributed ($\kappa = \frac{1}{3}$). Whatever the average angle of orientation of the collagen fibres, the minimum value of the resistance of the composite tissue is recorded when the collagen fibres are uniformly dispersed. This situation corresponds well to the case of aneurysmal tissue which presents a maximum risk of rupture.

So, the most significant cases of maximum resistance are obtained for the orthotropic case ($\kappa = 0$) of the composite tissue precisely, when all the CFs are aligned according to the

circumferential direction (e_T), i.e., $\theta = 0^\circ$, but the minimum of σ_T is obtained for orthotropic case ($\kappa = 0$) when all the fibres are longitudinally oriented, ie $\theta = 90^\circ$.

Also, it is observed that a decrease in the resistance of the aneurysmal tissue is obtained for an increase in κ whatever the angle value of average orientation of the CFs as shown in Fig. 8.

So, whatever the fibre orientation (θ), the stress σ_T reaches its minimum at $\kappa = \frac{1}{3}$ which corresponds to the isotropic case of diseased aortic tissue. In both cases of histological presentation ($\kappa = \frac{1}{3}$ et $\theta = 90^\circ$), the result is consistent with the observations reported in several experimental studies, including Zidi et al. (2014), Xiong et al. (2009), Gasser et al. (2006) and Niestrawska (2016) which announced the isotropy of the behavior of aneurysmal tissues.

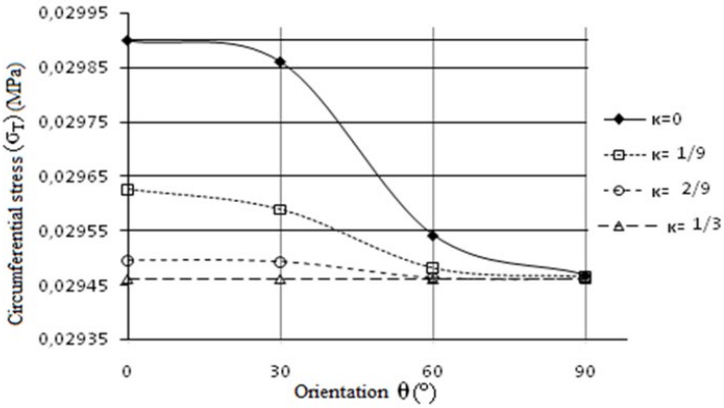

Fig. 7. Cauchy circumferential stress σ_T versus orientation angle θ of the AAA tissue; $(\kappa = 0, \frac{1}{9}, \frac{2}{9}, \frac{3}{9})$.

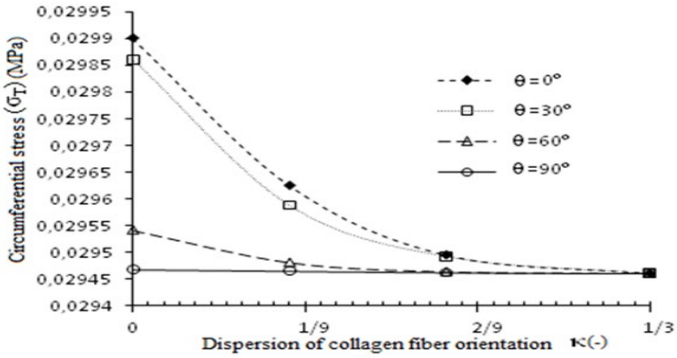

Fig. 8. Circumferential Cauchy stress σ_T as function of the dispersion κ (at different mean directions (θ) of the fibres).

4. Conclusion and recommendations

In this paper, to show the relationship between the weakness of the aneurismal wall and the pathological remodelling expressed by θ and κ, the following steps are considered:

a- AAA geometrical reconstruction from measured data collected during the aneurysm creation using xenograft technique in rats,

b- numerical simulations on the obtained geometrical model with different orientations, and dispersions using mechanical and micro-structural GOH model which can be decoupled in isotropic contribution of the base matrix and another orthotropic of the fibrous reinforcement where the density and the orientation of the FCs are expressed explicitly by the dispersion parameter κ and the direction angle θ.

c- Collection of the results and establishment of evolution curves $\sigma_T(\theta)$ and $\sigma_T(\kappa)$ that are shown in Fig. 7 and Fig. 8.

The results of the numerical simulation showed (see Figures 7 and 8) that it three different ranges of variations of the fibre orientation effect can be seen. In the first region (θ varies from 90° to 60°), the lowest values of σ_T are recorded, since the fibers are longitudinally directed involving a minimum contribution of collagen to circumferential resistance of the composite tissue. In the second region (θ varies from 30 to 60°), σ_T decreases drastically, showing an inflexion point around $\theta = 45°$ where the reinforcement acts simultaneously against the circumferential and longitudinal deformations. While in the last region (θ varies from 0° to 30°), the curves of (σ_T) decrease exponentially to converge towards its minimum value at $\theta = 90°$. That is valid for all values of the dispersion parameter. At this point, the fibrous reinforcement contribution vanishes in circumferential direction.

For the longitudinal orientation of all CFs ($\theta = 90°$), regardless of κ values (Fig.7), that suggests that the extracellular matrix represented in this study by the CFs intervenes to resist only against the longitudinal stretching λ_Z.

While the resistance to the circumferential tensions is in majority ensured by only the cellular matrix (SMC) when $\kappa = 0$. This makes the aneurismal wall circumferentially very weak with an important rupture risk factor by tangential stress. In an opposite manner, when ($\theta = 0°$), the CFs become circumferential and once straightened and stretched as defined in W_{aniso} of equation (10), they offer a maximum global resistance to the aortic wall as can be interpreted by equations (12 and 13).

These equations show that the strength of the aneurysmal tissue is provided by the superposition of the two histological matrixes contributions (CFs and SMC). In the case of an idealized cylindrical aortic wall, the wall stress tensor can be deduced according to the equations (12), (13) and (14) and can validate the numerical results reported previously in this paragraph.

Finally, it can be deduced that when aneurism as a disease causes a high dispersion in orientation of collagenous reinforcement, the tissue became isotropic ($\kappa = \frac{1}{3}$) with the lowest resistance in circumferential direction as mentioned in many experimental studies such as He (1994), Vande Geest (2006) and Zidi (2014).

In the present study, it was assumed that the fibres are arranged in the tangential plane in two families symmetrically disposed with respect to the circumferential axis, although in other studies such as Gasser (2006) and Niestrawska (2016), it has been reported that the aneurismal tissues

exhibited a collagenous network with a variable average symmetric and non-symmetric orientations between ($\theta = 0°$ to $\theta = 29°$).

So, we can conclude that the pathological weakness of the aneurysmal wall can result from the spatial disorganization of the fibrous reinforcement making its collagen fibres without any privileged orientation.

The study can help to better understand the effects of the aneurysm on the resistance of the arterial wall and from that better design vascular prostheses and more precisely target cellular therapies.

The results provided by this numerical study cannot be universal and require more experimental data on the microhistology of aneurysmal tissues. So, in order to be more realistic, the results of the present study must be obtained for a geometric model reconstructed on the basis of data collected at the date D(x) with an average direction and corresponding calculated dispersion of fibres that are observed with mechanical properties obtained at the same date.

References

Anidjar S, Salzmann JL, Gentric D, Lagneau P, Camilleri JP and Michel JB. (1990). Elastase-induced experimental aneurysms in rats. Circulation 82: 973-981.

AyyalasomayajulaV, Pierrat B and Badel, P. (2023). Failure properties and microstructure of porcine aortic adventitia: fiber level damage vs tissue failure. bioRxiv, 2023-03.

Di Martino ES, Bohra A, Vande Geest JP, Gupta NY, Makaroun MS and Vorp DA. (2006). Biomechanical properties of ruptured versus electively repaired abdominal aortic aneurysm wall tissue. J. Vasc. Surg. 43, 570–576.

Dingemans KP, Teeling JH, Lagendijk JH and Becker AE. (2000). Extracellular Matrix of the Human Aortic Media: An Ultrastructural histochemical and Immunohistochemical Study of the Adult Aortic Media. The anatomical record 258, 1–14.

Djellouli D, Naïm J, Bouaricha A, Bouchelaghem A and Zidi M. (2017). Etude du comportement mécanique de l'anévrisme de l'aorte abdominale créé par le modèle de xénogreffe de rat. Revue des composites et des matériaux avancés 27(1-2), 45-56.

Dobrin PB. (1989). Pathophysiology and pathogenesis of aortic aneurysms. Current concepts. Surgical Clinics of North America 69, 687-703.

Fillinger MF, Marra SP, Raghavan ML and Kennedy FE. (2003) Prediction of rupture risk in abdominal aortic aneurysm during observation: wall stress versus diameter. J. Vasc. Surg. 37, 724–732.

Fonck E, Prod'hom G, Roy S, Augsburger L, Rufenacht DA and Stergiopulos N. (2007). Effect of elastin degradation on carotid wall mechanics as assessed by a constituent-based biomechanical model. American. Journal of Physiol. Heart Circ. Physiol. 292, H2754–H2763.

Gasser TC, Ogden RW and Holzapfel GA. (2006). Hyperelastic modelling of arterial layers with distributed collagen fibre orientations. J. R. Soc. Interface 3, 15–35.

He CM, Roach MR. (1994). The composition and mechanical properties of abdominal aortic aneurysms. J. Vasc. Surg. 20, 6–13.

Holzapfel GA. (2000). Biomechanics of Soft Tissue. Handbook of material behavior non linear models and properties edited by Jean Lemaitre, LMT- Cachan, France.

Hariton I., Debotton G., Gasser T.C. and Holzapfel, G.A. (2007). Stress driven collagen fibre remodeling in arterial walls. Biomech. Model. Mechanobiol. 6 (3), 163–175.

JF Eberth, L. Cardamone and J.D. Humphrey (2011). Evolving biaxial mechanical properties of mouse carotid arteries in hypertension. Biomech. 2011 September 23; 44(14): 2532–2537.

Jonathan P.Vande Geest David A.Vorp (2006). The effects of aneurysm on the biaxial mechanical behavior of human abdominal aorta, Journal of Biomechanics. Pages 1324-1334.

Lindeman, J.H.N.; Ashcroft, B.A.; Beenakker, J.W.M.; Es, M. van; Koekkoek, N.B.R.; Prins, F.A.; Tielemans, J.F. Abdul-Hussien, H.; Bank, R.A.; Oosterkamp, T.H. (2010). Distinct defects in collagen microarchitecture underlie vessel-wall failure in advanced abdominal aneurysms and aneurysms in Marfan syndrome. Proceedings of the National Academy of Sciences. 107 (2), 8062-65.

Niestrawska JA, Viertler C, Regitnig P, Cohnert TU, Sommer G, Holzapfel GA. (2016). Microstructure and mechanics of healthy and aneurysmatic abdominal aortas: experimental analysis and modelling. J. R. Soc. Interface 13: 20160620.

Polzer S, Gasser CT, Bursa J, Staffa R, Vlachovsky R, Man V, Skacel P. (2013). Importance of material model in wall stress prediction in abdominal aortic aneurysms. Med Eng Phys. 35:1282–1289.

Roach, M. R. and Burton, A. C. (1957). The reason for the shape of distensibility curves of arteries, Canadian Journal of biochemistry and physiology 35(8): 681-690.

Rodríguez JF. Ruiz C. Doblaré M. Holzapfel GA. (2008). Mechanical stresses in abdominal aortic aneurysms:influence of diameter, asymmetry and material anisotropy. Biomech Eng. 130: 021023-1–10

Rodríguez JF, Martufi G, Doblaré M, Finol EA. (2009). The effect of material model formulation in the stress analysis of abdominal aortic aneurysms. Ann Biomed Eng. 37:2218–2221.

Sakalihasan, N., Limet, R., Defawe, O., (2005). Abdominal aortic aneurysm. Lancet 365, 1577–1589.

Tedgui A, Lévy B. (1994). Biologie de la paroi artérielle - aspects normaux et pathologiques. Masson, Paris

Tsamis, A., Phillippi, J. A., Koch, R. G., Pasta, S., D'Amore, A., Watkins, S. C., & Vorp, D. A. (2013). Fibre micro-architecture in the longitudinal-radial and circumferential-radial planes of ascending thoracic aortic aneurysm media. Journal of biomechanics, 46(16), 2787-2794.

Vande Geest J. P., Sacks M. S., Vorp D. A. (2006). The effects of aneurysm on the biaxial mechanical behavior of human abdominal aorta. J Biomech;39(7):1324-34.

Wang X, LeMaitre SA, Chen L, Shen YH, Gan Y. (2006). Increased Collagen Deposition and Elevated Expression of Connective Tissue Growth Factor in Human Thoracic Aortic Dissection. Circulation114, I-200–I-205.

Watton PN, Hill NA. (2009). Evolving mechanical properties of model of Abdominal aortic aneurysm. Biomechanical Modeling Mechanobiol 8, 25-42

Xiong W, Knispel R, Mactaggart J, Greiner TC, Weiss SJ, Baxter B T. (2009). Membrane-type 1 matrix metalloproteinase regulates macrophage-dependent elastolytic activity and aneurysm formation in vivo. Journal Biol Chem 284, 1765-1771.

Zidi M, Allaire E. (2014). Mechanical behavior of abdominal aorta aneurysm in rat model treated by cell therapy using mesenchymal stem cells. Biomechanical Model Mechanobiol. 14, no 1, 185-194.

Zulliger, M. A., & Stergiopulos, N. (2007). Structural strain energy function applied to the ageing of the human aorta. Journal of biomechanics, 40(14), 3061-3069.